The phase mismatch ϑ, including nonlinear terms, is

$$\vartheta = (2\beta_P - \beta_A - \beta_S) - (3P_A + 6P_P + 6P_S)\frac{n_2\omega_A}{2cnA_{eff}}\ m^{-1} \quad (4)$$

where ω_A is the angular frequency of the anti-Stokes light, n is the refractive index, c is the velocity of light in vacuum, n_2 is the nonlinear refractive index of hydrogen, and the linear wavevectors are $\beta_i = \omega_i n_i/c$ (including the dispersion of the gas and the waveguide). For our experimental parameters ($P_P \sim P_S \sim 100$ W, $n = 1$, resonant $n_2 = 1.2' 10^{-17}$ m^2/W, an interaction length $L \sim 0.1$ m, and $A_{eff} = 150$ μm^2), we obtain $P_A = 3 \times 10^4 \sin c^2(\vartheta L)$W. Evaluation of the phase mismatch assuming (as a rough approximation) perfect metallic boundary conditions at the core boundary (*12*) yields $\vartheta L \sim 1000$ (the nonlinear term is negligible), which when taking the peaks of the sin c^2 function yields $P_A \sim 0.04$ W, which is some 25 times smaller than the experimental measurement of 1 W.

Equation 3 also shows that even under exact phase matching, the anti-Stokes power will increase only as the square of distance. In the data, however, the rate of growth is much faster. Indeed, the ratio $P_A/(zP_P\sqrt{P_S})^2$, which might be expected to be constant for perfect phase matching ($\vartheta = 0$), actually increases exponentially with distance in the experiments. This could be explained through a self-focusing phenomenon that reduces the effective area so as to enhance the four-wave mixing process and the phase matching. What is clear is that we are operating in a new parameter regime of extremely high, well-controlled Stokes and pump intensities over long interaction distances.

After peaking at $z \sim 35$ cm, the Stokes signal drops strongly, as already discussed. At the same time, the anti-Stokes power drops at a rate of only ~2 dB/m; that is, less quickly than the intrinsic linear attenuation (3 dB/m) of the HC-PCF, suggesting that some anti-Stokes gain is still present. Finally, at $z > 55$ cm, the attenuation of all three components settles down to ~3 dB/m, corresponding to the linear loss of the HC-PCF.

The highest observed Stokes conversion efficiency was 30 ± 3%, occurring at $z = 32$ cm and $E_c = 4.5$ μJ. The conversion efficiency is evidently limited by the strong, nonlinear, loss self-focusing mechanism. At both $z = 17$ and 56 cm, the highest efficiencies occurred at $E_c \sim 3.5$ μJ, taking the values ~14 and 0.8%, respectively.

The reduction in threshold power for gas-SRS should allow the use of low-power solid-state diode-pumped lasers as pumps and should extend the wavelengths of solid-state sources into new spectral regions. Further orders-of-magnitude reductions in pump source requirements will follow from dispersion management and improvement of fiber performance. A narrower line laser source would lead to further improvements in performance. The possibility of setting a linear gradient of the pressure along the fiber might be useful for pulse chirping (*16*). The ability to load HC-PCF at high pressure without damage could also be of great importance for SRS in the transient regime (that is, when the pulse duration is much shorter than the dephasing time), where the Raman gain is proportional to the pressure (*17*).

The availability of HC-PCF is likely also to lead to rapid new progress in all types of nonlinear optics in gases and should mark the beginning of a new era in gas-based nonlinear optics.

References and Notes

1. R. F. Cregan *et al.*, *Science* **285**, 1537 (1999).
2. T. A. Birks, P. J. Roberts, P. St. J. Russell, D. M. Atkin, T. J. Shepherd, *Electron. Lett.* **31**, 1941 (1995).
3. P. Rabinowitz *et al.*, *Appl. Opt.* **15**, 2005 (1976).
4. L. S. Meng *et al.*, *Opt. Lett.* **25**, 472 (2000).
5. M. J. Renn, R. Pastel, *J. Vac. Sci. Technol. B* **16**, 3859 (1998).
6. S. E. Harris, A. V. Sokolov, *Phys. Rev. Lett.* **81**, 2894 (1998).
7. A. V. Sokolov, D. D. Yavuz, S. E. Harris, *Opt. Lett.* **24**, 557 (1999).
8. R. W. Hellwarth, *J. Opt. Sci. Am.* **68**, 1050 (1978).
9. The mode profiles of the guided modes in HC-PCF match very well with the modes in a hollow waveguide made from a perfect metal [see, for example, J. A. West *et al.*, in *Proceedings of the 26th European Conference on Optical Communication*, (VDE Verlag, Berlin, 2000), vol. 4, pp. 41–42]. The lowest-order mode has a Bessel-like modal field profile, which is strongly confined in the air core.
10. J. C. Knight *et al.*, *Opt. Lett.* **21**, 1547 (1996).
11. K. Suzuki, M. Nakazawa, "Ultrabroad band white light generation from multimode photonic bandgap fiber with an air core," paper presented at the Conference on Lasers and Electro-Optics/Pacific Rim, Chiba, Japan, 15 to 19 July 2002.
12. J. A. West, N. Venkataramam, C. M. Smith, M. T. Gallagher, in *Proceedings of the 27th European Conference on Optical Communication*, 26 September to 4 October 2001, Amsterdam, vols. 1 to 6, pp. 582–585.
13. This is partially due to the large linewidth of our laser (3 cm^{-1}) compared with the Raman linewidth <0.03 cm^{-1}.
14. Y. R. Shen, *The Principles of Nonlinear Optics* (Wiley, New York, 1984).
15. G. Tempea, T. Brabec, *Opt. Lett.* **23**, 762 (1998).
16. A. Rundquist *et al.*, *Science* **280**, 1412 (1998).
17. S. E. Harris, A. V. Sokolov, *Phys. Rev. A* **55**, R4019 (1997).

18. We thank A. George for technical support in the design and the construction of the gas cells.

22 July 2002; accepted 28 August 2002

Rapid Vapor Deposition of Highly Conformal Silica Nanolaminates

Dennis Hausmann, Jill Becker, Shenglong Wang, Roy G. Gordon*

Highly uniform and conformal coatings can be made by the alternating exposures of a surface to vapors of two reactants, in a process commonly called atomic layer deposition (ALD). The application of ALD has, however, been limited because of slow deposition rates, with a theoretical maximum of one monolayer per cycle. We show that alternating exposure of a surface to vapors of trimethylaluminum and tris(*tert*-butoxy)silanol deposits highly conformal layers of amorphous silicon dioxide and aluminum oxide nanolaminates at rates of 12 nanometers (more than 32 monolayers) per cycle. This process allows for the uniform lining or filling of long, narrow holes. We propose that these ALD layers grow by a previously unknown catalytic mechanism that also operates during the rapid ALD of many other metal silicates. This process should allow improved production of many devices, such as trench insulation between transistors in microelectronics, planar waveguides, microelectromechanical structures, multilayer optical filters, and protective layers against diffusion, oxidation, or corrosion.

Thin films are ubiquitous in modern technology. For example, processing, storage, and communication of information rely on a wide variety of thin films of semiconductors, metals, and insulators. Many different methods are used to make these films, such as various physical techniques (e.g., sputtering, evaporation, pulsed laser ablation) and chemical processes (e.g., oxidation, chemical vapor deposition, electroplating, sol-gel synthesis) (*1*).

Assembling thin films atom by atom allows exquisite control over their composition and structure. One such technique is atomic layer deposition (ALD; also called atomic layer epitaxy), in which a vapor reacts with a surface until a monolayer has been chemisorbed (*2*). The reaction then stops, so the process is called "self-limiting." A second vapor then reacts with this surface in a second self-limiting reaction, thus depositing a second layer of atoms onto the

Department of Chemistry and Chemical Biology, Harvard University, 12 Oxford Street, Cambridge, MA 02138, USA.

*To whom correspondence should be addressed. E-mail: gordon@chemistry.harvard.edu

first. The second reaction must also return the surface to a state in which it is ready to react with the first reactant. The cycle of reactions can then be repeated to build up a binary compound atomic layer by atomic layer. Additional reactants having suitably complementary self-limiting reactions can be used to form ternary compounds, doped compounds, graded compositions, or nanolaminates showing properties that are dramatically improved over homogeneous materials (*3, 4*).

ALD offers a number of other remarkable capabilities in addition to the control of stoichiometry at an atomic level. The thickness of a film can be set digitally by counting the number of reaction cycles and is substantially immune to variations caused by nonuniform distribution of vapor or temperature in the reaction zone. Thus, uniformly thick coatings can easily be deposited over large areas and over convoluted geometries, such as inside very narrow holes (*5*). ALD is an established technique for the production of large-area electroluminescent displays (*6*). The silicon semiconductor industry is currently devoting a large amount of research to ALD as a likely future method for the production of very thin films needed in microelectronics (*7*). Many other potential applications of ALD are, however, discouraged by its low deposition rate, typically <0.2 nm (less than half a monolayer) per cycle. Previously known reactions for ALD of silica are particularly slow (*8–15*), requiring >1 min to complete a reaction cycle. We report on an ALD reaction that deposits dozens of monolayers in each cycle that is <30 s long, resulting in a deposition rate that is >100 times the rate of previously known ALD reactions for silica. Current theoretical understanding (*16–18*) is incompatible with such a large cycle thickness.

Vapors doses of trimethylaluminum (Me_3Al) (*19*) and tris(*tert*-butoxy)silanol [$(Bu^tO)_3SiOH$] (*20*) were supplied (*21*) in alternating pulses to heated surfaces (*22*) on which transparent, smooth (*23*) films of alumina-doped silica (*24*) grew. Control experiments with only one or the other of the reactants alone produced no deposition. The thickness (*25*) was linear in the number of pairs of doses ("cycles"). The thickness per cycle depended on the sizes of the doses and on the substrate temperature, as shown in Fig. 1, reaching the high value of 12 nm/cycle.

The self-limiting character of these two surface reactions is demonstrated by the saturation of the growth rate at high doses of each reactant in Fig. 1, A and B. For doses in the saturated range, the films have highly uniform thickness, even though the vapors flow nonuniformly toward the surface of the substrate, entering from one end of the reactor tube. For doses smaller than the saturated range, the films have the saturated thickness only partway along the length of the tube and then become thinner where the vapor is depleted near the exit end of the tube (*26*). At temperatures <200°C and >300°C, the film thickness was not uniform over any region of the deposition zone. A summary of the saturated deposition rates is shown in Fig. 1C. The highest saturated deposition rates were found at substrate temperatures between 225° and 250°C.

Additional evidence for the self-limiting, saturating behavior of the two surface reactions comes from real-time measurements of mass deposited on a quartz crystal microbalance (*27*) inserted into the deposition zone. The curve in Fig. 2 shows the mass gains as each of 60 small, nonsaturating doses of $(Bu^tO)_3SiOH$ (silanol) was introduced. The earlier mass gains are larger; they decrease in size as saturation is approached. Thus, the reactive sticking coefficient decreases as the layer reaches its limiting thickness. According to the data in Fig. 1A, ~80 of these small doses would have been required for complete saturation to be reached.

The uniformity of coatings inside deep, narrow holes is an extremely sensitive test of whether a pair of ALD reactions saturate by a self-limiting mechanism. Accordingly, films were deposited on a silicon wafer in which deep, narrow holes had previously been etched. After depositing four ALD cycles, the wafer was cleaved, and cross-sectional scanning electron micrographs (SEMs) were recorded. The images in Fig. 3 show uniform (*28*), conformal coating indicative of an ideal self-limiting ALD reaction. Nine cycles completely filled holes 0.2 μm in diameter.

The composition of the films is stoichiometric silicon dioxide (SiO_2), along with ~0.6 atomic % of aluminum. Carbon was not detected in the films (<0.3 atomic %). The films are amorphous by x-ray and electron diffraction (*29*). The film density is 2.0 g/cm^3, which is ~91% of the value for bulk fused (amorphous) silica. The structure of these conformal silica films can be described as a nanolaminate, in which very thin layers of alumina are interspersed between thicker layers of silica. The nanolaminate structure can be visualized by SEMs of a cleaved and etched surface, which shows faint horizontal striations with the expected periodicity in the vertical direction (Fig. 4). Many optical, electrical, and mechanical properties of the silica are hardly changed by the presence of the small amount of alumina. The refractive index, dielectric constant, leakage current, and breakdown voltage are similar to values measured (*30*) for pure silica films grown thermally on silicon. However, some properties,

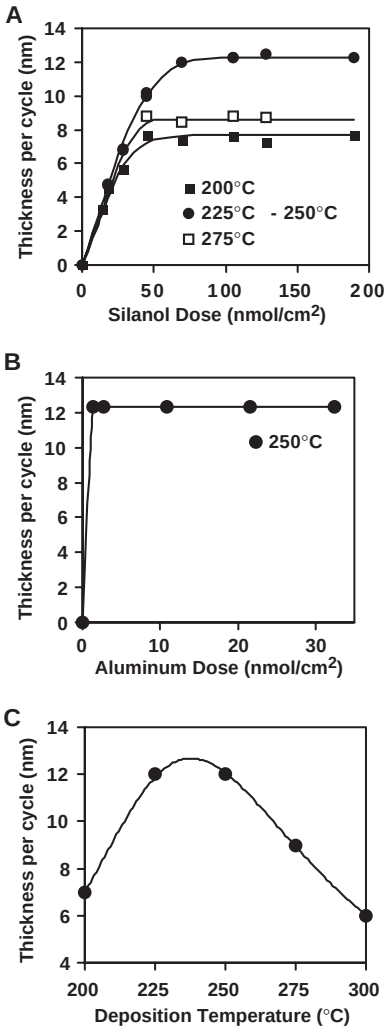

Fig. 1. Growth rate (in nm/cycle) as a function of (**A**) $(Bu^t O)_3SiOH$ dose and (**B**) Me_3Al dose. (**C**) Saturated ALD growth rates of silica (in nm/cycle) as a function of substrate temperature. The points are the experimental data; the line represents the kinetic model.

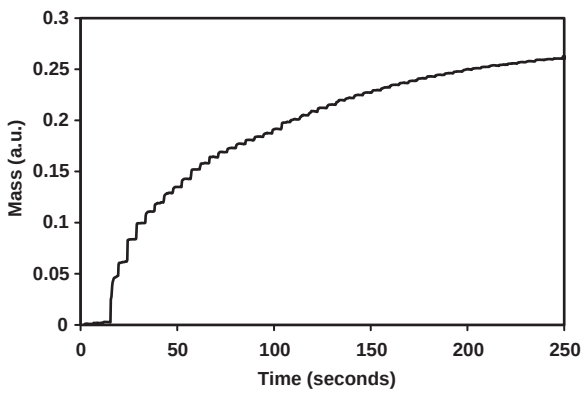

Fig. 2. Mass changes recorded by a quartz crystal microbalance at 250°C following 60 undersaturating doses of 1 nmol/cm^2 of $(Bu^tO)_3SiOH$. Before the first $(Bu^tO)_3SiOH$ dose, Me_3Al was introduced and purged out of the reactor. Each dose is separated by 4 s of nitrogen purging. a.u., arbitrary units.

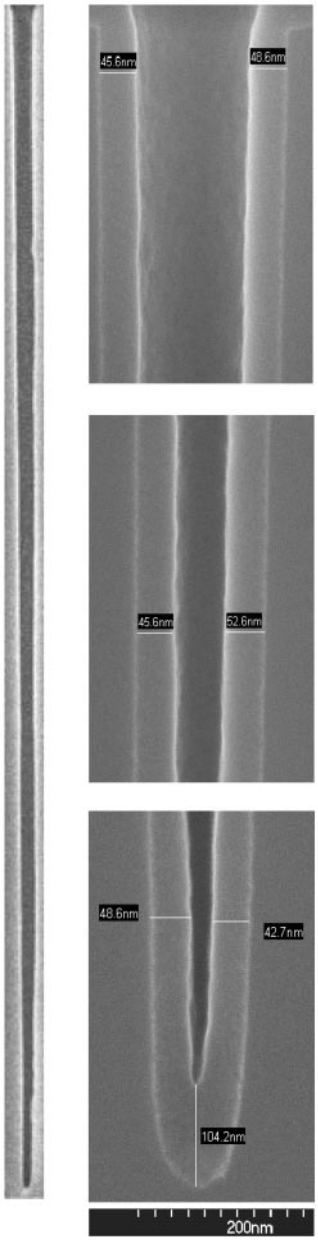

Fig. 3. Cross sections of holes 7 μm deep and 0.1 to 0.2 μm in diameter. On the left is a complete uncoated hole. On the right are higher magnification images of the top, middle, and bottom of a hole coated conformally with a uniform silica film 46 nm thick made by four ALD cycles.

such as resistance to atomic diffusion and electrical breakdown voltage, can be increased by carrying out several ALD alumina cycles (Me_3Al then H_2O) before repeating each dose of silanol.

Because a monolayer of silica is ~0.37 nm thick (*31*), each cycle of the deposition process deposits >32 monolayers. We propose a mechanism to account for the unexpectedly large thickness of these self-limited layers. Studies (*32–34*) of the first half-reaction of Me_3Al with hydroxylated surfaces have concluded that one of the chemisorption reactions is that shown in

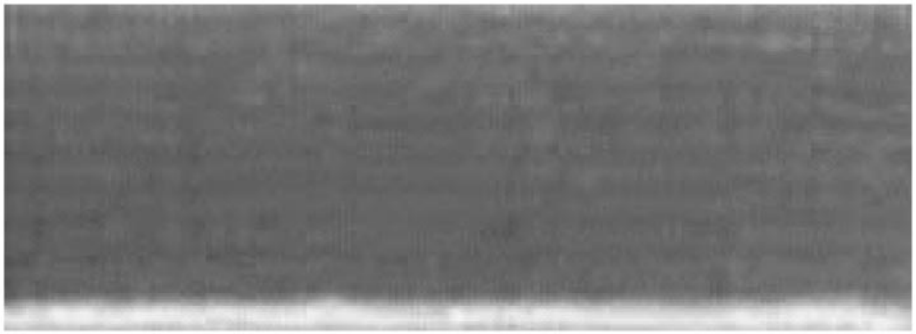

Fig. 4. SEM of a cleaved and etched cross section of a silica and alumina nanolaminate film. The bright band at the bottom is the substrate. The periodicity of the horizontal bands matches the cycle thickness of 12 nm.

Scheme 1A. The $(Bu^tO)_3SiOH$ then chemisorbs onto this methylaluminum-containing surface during the second half-reaction, again eliminating methane (Scheme 1B). Additional silanol molecules can then diffuse down to the surface and insert into the aluminum-oxygen bonds by a concerted mechanism (Scheme 1C).

Repeated insertions of silanol into the aluminum-oxygen bond form a siloxane polymer bound to the surface through the aluminum (Scheme 1D) (*35*). This siloxane polymer is attached to the surface by strong chemical bonds and thus is nonvolatile; the conversion of the volatile silanol to nonvolatile siloxane polymer is an irreversible chemisorption process. Because the silanol can diffuse through this soft, surface-bound siloxane polymer, the aluminum atoms remain available to catalyze the polymerization of more silanol molecules. The rate-limiting step in this process is the catalytic conversion of silanol to siloxane, provided that the concentration of silanol vapor is sufficiently high to keep the catalytic aluminum atoms fully occupied. In this case, the chemisorption rate does not depend on the rate at which silanol arrives at the surface of the siloxane layer. In the language of chemical kinetics, the chemisorption rate is zero order in the vapor concentration of silanol. This condition is important in making uniformly thick films, independent of nonuniformities in the distribution of silanol vapor over the surface.

The self-limiting nature of the ALD reaction results from cross-linking of the siloxane polymer, according to the following reactions. First, the *tert*-butyl groups on the siloxane thermally decompose through β-hydrogen elimination of isobutene (Scheme 1E), leaving hydroxyl groups on the silicon (*36, 37*). A newly formed hydroxyl group may transfer a hydrogen atom to a nearby butoxy group, eliminating *tert*-butanol and cross-linking the silicons by an oxygen atom (Scheme 1F). Cross-linking may also be achieved by the elimination of water between two adjacent hydroxyl groups (Scheme 1G).

These cross-linking reactions connect the siloxane polymer chains, causing the polymer layer to gel and eventually solidify to silica (SiO_2). Because the silanol presumably has a negligible rate of diffusion through solid silica, additional silanol can no longer reach the catalytic aluminum atoms, so the chemisorption of silanol finally stops (becomes self-limited). Sufficient hydroxyl groups remain on the surface of the silica, so that the cycle may begin again by reaction with the next dose of Me_3Al.

The only volatile by-products detected were isobutene, *tert*-butanol, and water, in qualitative agreement with the proposed mechanism. (Methane was not retained in the liquid nitrogen trap.) To test whether the hydroxyl group in the silanol is essential to this mechanism, we conducted a control experiment, in which the $(Bu^tO)_3SiOH$ was replaced with tetra(*tert*-butoxy)silane $[(Bu^tO)_4Si]$ (*38*). No film was formed on substrates at the temperatures tested (up to 450°C), confirming that the hydroxyl group in $(Bu^tO)_3SiOH$ is a critical factor in its high reactivity. Bis(*tert*-butoxy)silanediol $[(Bu^tO)_2Si(OH)_2]$ (*39*) did form films, in agreement with this conclusion.

The question also arises as to whether the aluminum-carbon bonds on the initial surface play an essential role. Therefore, we performed another series of depositions, in which a dose of water vapor was introduced after the Me_3Al dose and before the silanol dose. Water is known to replace aluminum-methyl bonds with aluminum-hydroxyl bonds (*32–34*). The resulting films were identical to those made without the water dose. Identical results were obtained from another test with ALD of aluminum dimethylamide $[Al_2(NMe_2)_6]$ in place of the Me_3Al and water to form an aluminum-containing surface. We conclude that the mechanism is not very specific in its requirements for particular ligands on the aluminum. Rather, it seems only to depend on the presence of aluminum atoms on the surface after the first half-reaction.

Quantum chemical calculations (*40*) were done for the insertion of $(Bu^tO)_3SiOH$ into an aluminum-oxygen bond (*41*), according to Scheme 1C. A low-energy transition state was found with energy essentially equal to

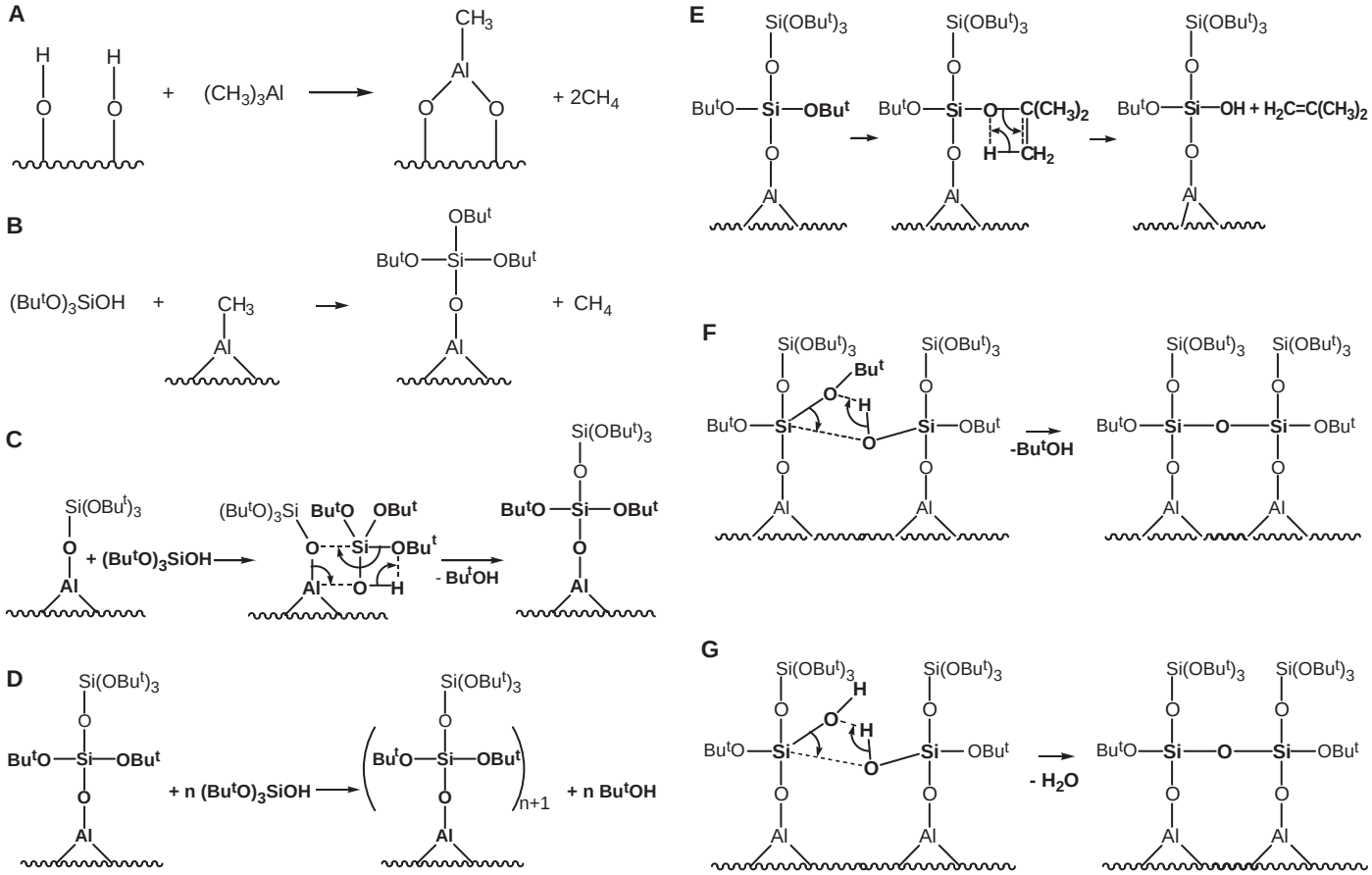

Scheme 1.

that of the reactants, demonstrating that this concerted reaction can be facile. Nevertheless, a modest activation energy of 74 kJ/mol is predicted for this insertion reaction because the reactants form a complex bound by this amount of energy. For comparison, the uncatalyzed elimination of *tert*-butanol has a much higher activation energy of 197 kJ/mol.

The predicted 74 kJ/mol activation energy for the aluminum-catalyzed reaction (Scheme 1, C and D) helps explain why the thickness per cycle increases as the deposition temperature increases from 200° to 225°C (Fig. 1, A and C). For substrates at temperatures >250°C, the thickness per cycle decreases because the reaction becomes self-limited in a shorter time. This occurs because some of the condensation reactions leading to solid silica become faster. Between 225° and 250°C, these two competing temperature effects cancel, so the thickness per cycle is nearly constant as it passes through a maximum. The film thickness is extremely uniform (variation within the accuracy of measurement, ±0.5%) for substrates held at temperatures between 225° and 250°C, because the thickness is nearly independent of small temperature variations in the deposition zone.

A quantitative kinetic model was constructed from this mechanism. The theoretical activation energy was used for the catalytic polymerization step. The termination rate was assumed to be determined by the cross-linking of the polymer by two parallel reactions (Scheme 1, F and G). One of them was assumed to have negligible activation energy, and the activation energy and preexponential factor for the other cross-linking reaction were adjusted to find the good fit to the experimental data shown in Fig. 1C [growth rate = $(1.19 \times 10^9 e^{-74/RT})/(1 + 4 \times 10^{12} e^{-121/RT})$ nm/cycle, where R is the ideal gas constant in kJ/mol·K and T is the temperature in kelvin].

Thus, the unusual temperature dependence of the reaction rate can be understood with the proposed mechanism. The kinetic model also helps to explain why ALD growth was not found outside the temperature range of 200° to 300°C. At temperatures >300°C, the rate of polymerization is so fast that the catalytic aluminum centers cannot be kept fully occupied with silanol. The growth rate becomes flux dependent, and the thickness varies along the reactor tube because of the nonuniform distribution of silanol vapor. At temperatures <200°C, the deposition is not self-limited because the cross-linking of the polymer is too slow to be completed during the silanol part of the cycle (15 s). Quartz crystal microbalance data show that the reaction of Me_3Al is complete within its time resolution of 0.2 s.

Because the catalytic mechanism depends mainly on the Lewis acid character of the aluminum, we expect that many other metals should show a similar catalytic activity. In similar experiments on ALD of lanthanum, zirconium, and hafnium silicates, we also found deposition rates that are too large to be understood by traditional theories without a catalytic mechanism (*42*).

We conclude that the alternating surface reactions of Me_3Al and $(Bu^tO)_3SiOH$ vapors form silica nanolaminates >32 atomic layers thick in a single cycle. We refer to our reaction cycle by the general term "alternating layer deposition" to describe the multilayer growth observed in a single cycle. Because of its increased deposition rate and extreme conformality, we expect that alternating layer deposition will find many applications.

References and Notes

1. For an introductory survey of these methods, see D. L. Smith, *Thin Film Deposition: Principles and Practice* (McGraw-Hill, New York, 1995).
2. For a recent review of ALD, see M. Ritala, M. Leskela, in *Deposition and Processing*, vol. 1 of *Handbook of Thin Film Materials*, H. S. Nalwa, Ed. (Academic Press, San Diego, CA, 2002), pp. 103–159.
3. H. Zhang, R. Solanki, *J. Electrochem. Soc.* **148**, F63 (2001).
4. K. Kukli, J. Ihanus, M. Ritala, M. Leskela, *J. Electrochem. Soc.* **144**, 300 (1997).
5. A. E. Braun, *Semicond. Int.* **24**, 52 (2001).
6. T. Suntola, M. Simpson, Eds., *Atomic Layer Epitaxy* (Blackie, London, 1990).

7. A. I. Kingon, J.-P Maria, S. K. Streiffer, *Nature* **406**, 1032 (2000).
8. S. M. George *et al.*, *Appl. Surf. Sci.* **82–83**, 460 (1994).
9. W. Gasser, Y. Uchida, M. Matsumura, *Thin Solid Films* **250**, 213 (1994).
10. S. Morishita, W. Gasser, K. Usami, M. Matsumura, *J. Non-Cryst. Solids* **187**, 66 (1995).
11. K. Yamaguchi *et al.*, *Appl. Surf. Sci.* **130–132**, 202 (1998).
12. J. W. Klaus, O. Sneh, A. W. Ott, S. M. George, *Surf. Rev. Lett.* **6**, 435 (1999).
13. J. D. Ferguson, A. W. Weimer, S. M. George, *Appl. Surf. Sci.* **162–163**, 280 (2000).
14. _____, *Chem. Mater.* **12**, 3472 (2000).
15. J. W. Klaus, S. M. George, *Surf. Sci.* **447**, 81 (2000).
16. M. Ylilammi, *Thin Solid Films* **279**, 124 (1996).
17. J.-W. Lim, J.-S. Park, S.-W. Kang, *J. Appl. Phys.* **87**, 4632 (2000).
18. J.-S. Min *et al.*, *Jpn. J. Appl. Phys., Part 1* **37**, 4999 (1998).
19. Me_3Al from Albemarle Corporation (Baton Rouge, LA) was held at 25°C, at which temperature its vapor pressure is ~15 torr.
20. This was prepared by the method described in (*43*) and also obtained from Aldrich Chemical Company (Milwaukee, WI) and Gelest Inc. (Morrisville, PA) and heated to 115°C, at which temperature it has a vapor pressure of ~20 torr.
21. To deliver pulses of Me_3Al vapor, we opened a three-way valve, with inner channels of 0.4-mm inner diameter, to Me_3Al vapor for 1 s, during which time 1 μmol of Me_3Al vapor flowed into the deposition chamber. Then, the three-way valve was turned to flow nitrogen for 5 s to purge the chamber of residual unreacted Me_3Al vapor. To deliver $(Bu^tO)_3SiOH$ vapor, we filled a 35-ml volume with $(Bu^tO)_3SiOH$ vapor at its equilibrium vapor pressure (ranging from 3.1 to 100 torr at reservoir temperatures from 80° to 150°C). A valve between the deposition chamber and the vacuum pump was closed, and a valve between the 35-ml volume and the deposition chamber was opened to allow the measured dose of $(Bu^tO)_3SiOH$ vapor to expand into the deposition chamber. After 15 s, the valve to the pump was opened, and nitrogen was flowed for 5 s to purge the chamber of excess $(Bu^tO)_3SiOH$, as well as of volatile by-products of the reaction. This cycle was then repeated. At the end of the prescribed number of cycles (typically 4 to 100), substrates of silicon, glass, and glassy carbon were removed from the reactor. Identical results were found for other experiments in which the 15-s exposure time to $(Bu^tO)_3SiOH$ was increased to 90 s.
22. Silicon substrates were prepared by removing the native oxide with dilute hydrofluoric acid solution. Then the substrates were irradiated with ultraviolet light (from a mercury lamp) in air until the surface became hydrophilic (normally a couple of minutes).
23. Roughness measurements by atomic force microscopy [Digital Instruments (Santa Barbara, CA) and ThermoMicroscopes (Sunnyvale, CA)] showed that the films are just as smooth as their substrates.
24. Composition and number of atoms per unit area were determined by Rutherford backscattering spectroscopy [General Ionics Model 4117, 1.7 MeV Tandetron (Coyahoga Falls, OH)] of samples grown on glassy carbon substrates.
25. Thickness and refractive index were determined by ellipsometry [Rudolf Auto-El II (Flanders, NJ)]. Thickness and density were also found by low-angle x-ray reflection [Scintag Model XDS2000 (Cupertino, CA)].
26. In Fig. 1, the film thicknesses plotted for the underdosed experiments are the average over the whole length (30 cm) of the reactor tube. The film thickness near the entry point for the vapors still has the saturated value even for the underdosed conditions.
27. The microbalance used was an Inficon Technologies (East Syracuse, NY) bakeable quartz crystal microbalance.
28. The coating is uniform within the measurement accuracy of about ±3 nm for SEMs on a cleaved cross section.
29. X-ray scattering (Scintag Model XDS2000) and electron diffraction by transmission electron microscopy [JEOL 2010F (Peabody, MA)] determined that the films are amorphous.
30. Measured on capacitors formed by e-beam evaporation of platinum dots through a shadow mask.
31. This estimate of a monolayer thickness was obtained by taking the cube root of the volume occupied by a formula unit of SiO_2 in material with density of 2.0 g/cm^3.
32. A. C. Dillon, A. W. Ott, J. D. Way, S. M. George, *Surf. Sci.* **322**, 230 (1995).
33. M. Juppo, A. Rahtu, M. Ritala, M. Leskela, *Langmuir* **16**, 4034 (2000).
34. A. Rahtu, T. Alaranta, M. Ritala, *Langmuir* **17**, 6506 (2001).
35. A reaction that may be somewhat analogous to this step is the polymerization of a different silanol in solution as reported in (*44*).
36. K. W. Terry, P. K. Ganzel, T. D. Tilley, *Chem. Mater.* **4**, 1290 (1992).
37. C. G. Lugmair, K. L. Fujdala, T. D. Tilley, *Chem. Mater.* **14**, 888 (2002).
38. M. G. Voronkov, A. N. Lazarev, A. K. Baigozhin, *Zh. Obshch. Khim.* **26**, 3072 (1956) (Engl. transl., p. 3421).
39. G. Schott, L. Engelbrecht, H. J. Holdt, *Z. Anorg. Allg. Chem.* **459**, 177 (1979).
40. M. J. Frisch *et al.*, Gaussian 98 (Revision A.9) (Gaussian Inc., Pittsburgh, PA, 1998).
41. The system was simplified by using hydrogen atoms to terminate bonds that were more than two bonds away from the reaction center. The aluminum catalytic center was modeled as $Al(OH)_3$. On the $(Bu^tO)_3SiOH$, the two butoxy groups not involved in the initial chemisorption reaction are replaced by hydroxyl groups. The butoxy group that is initially cleaved as *tert*-butanol was simplified to a methyl group leaving as methanol. The structures and energies of the reactants, products, and transition state were calculated by the Gaussian program with density functional theory B3LYP using a very large basis set, 6-311++G(3df,3pd)//6-31+G(d).
42. R. G. Gordon, J. Becker, D. Hausmann, S. Suh, *Chem. Mater.* **13**, 2463 (2001).
43. Y. Abe, I. Kijima, *Bull. Chem. Soc. Jpn.* **42**, 1118 (1969).
44. J. H. Gaul, T. M. Carr, *Spec. Lett.* **16**, 651 (1983).

45. The etched wafer and the SEMs of the coated holes shown in Fig. 3 were supplied by M. Gutsche of Infineon Technologies (Munich, Germany). The SEM of the uncoated hole was taken by P. de Rouffignac. This work was supported in part by the NSF.

2 May 2002; accepted 9 September 2002

Role of ANC-1 in Tethering Nuclei to the Actin Cytoskeleton

Daniel A. Starr and Min Han*

Mutations in *anc-1* (nuclear anchorage defective) disrupt the positioning of nuclei and mitochondria in *Caenorhabditis elegans*. ANC-1 is shown to consist of mostly coiled regions with a nuclear envelope localization domain (called the KASH domain) and an actin-binding domain; this structure was conserved with the *Drosophila* protein Msp-300 and the mammalian Syne proteins. Antibodies against ANC-1 localized cytoplasmically and were enriched at the nuclear periphery in an UNC-84–dependent manner. Overexpression of the KASH domain or the actin-binding domain caused a dominant negative anchorage defect. Thus, ANC-1 may connect nuclei to the cytoskeleton by interacting with UNC-84 at the nuclear envelope and with actin in the cytoplasm.

A wide variety of organisms have syncytia, formed either when multiple nuclear divisions occur without cell divisions or when cells fuse together. Normally, syncytial nuclei are located in specific regions or are evenly spaced throughout the cytoplasm. Nuclear positioning is also essential to a variety of singlely nucleated polar cells and even in single-celled organisms (*1*). Microtubules and associated dynein and kinesin motors play a central role in the positioning of nuclei (*2*). Less is known about the role of actin in the process of nuclear positioning. However, a defect in the actin cytoskeleton of nurse cells of *Drosophila* oocytes disrupts nuclear anchorage during cytoplasmic dumping (*3*). Actin is also required for plant nuclear migrations (*4*). We used the large syncytial cells of *C. elegans* as a model to study the mechanism of nuclear anchorage. Most of the body of an adult worm is covered by four large syncytial hypodermal cells that contain more than 100 nuclei (*5*). Normally, nuclei are evenly spaced throughout the syncytia. However, mutations in either *anc-1* or *unc-84* cause an Anc phenotype, in which nuclei float freely within the cytoplasm of syncytial cells and often group together (*6*, *7*). The Anc phenotype is observed in all somatic, postembryonic syncytial cells, even in binucleated intestinal cells (*7*).

We determined the molecular identity of *anc-1* (*8*). RNA interference (RNAi) experiments and the identification of a molecular lesion in the predicted open reading frame of *anc-1(e1873)* confirmed that we had cloned *anc-1* (*8*) (Fig. 1, A to D, and fig. S1). The full-length cDNA of *anc-1* was predicted to be 25,639 base pairs (bp) encoding an 8546-residue protein. The bulk of ANC-1 (the *anc-1* gene product) consisted of mostly predicted coiled regions, including six repeats of 903 residues that are essentially identical at the nucleotide level (supporting online text). The length of the repeat region may be maintained because of a selective advantage of keeping ANC-1 large.

Howard Hughes Medical Institute and Department of Molecular, Cellular and Developmental Biology, University of Colorado, Boulder, CO 80309, USA.

*To whom correspondence should be addressed. E-mail: mhan@colorado.edu